applied sciences

MDPI

Article

Longitudinal Seismic Response of Continuously Welded Track on Railway Arch Bridges

Hao Liu [1,2], Ping Wang [1,2], Xiankui Wei [3], Jieling Xiao [1,2,*] and Rong Chen [1,2,*]

1 Key Laboratory of High-Speed Railway Engineering, Ministry of Education, Southwest Jiaotong University, Chengdu 610031, China; liuhao@my.swjtu.edu.cn (H.L.); wping@home.swjtu.edu.cn (P.W.)
2 School of Civil Engineering, Southwest Jiaotong University, Chengdu 610031, China
3 Chuannan Inter-City Railway Co., Ltd., Zigong Sichuan 643000, China; wei_xiankui@my.swjtu.edu.cn
* Correspondence: xjling@home.swjtu.edu.cn (J.X.); chenrong@home.swjtu.edu.cn (R.C.)

Received: 1 April 2018; Accepted: 9 May 2018; Published: 13 May 2018

Abstract: The seismic response of continuously welded track on bridges is seeing increased interest. Taking the railway deck arch bridge as an example, a track–bridge spatial coupling finite element model was established, and the effects of arch rib temperature difference and bridge span layout on rail seismic force were analyzed. The results show that the peak rail seismic force is larger than the maximum expansion force, and thus track constraints should be taken into consideration in railway arch bridge seismic design. The area enclosed by the hysteresis curve of track resistance increases gradually with an increase in dynamic displacement, and under seismic loading the track constraints can be considered to be in a relatively stable state of energy dissipation. The rail seismic forces under different waves varied greatly, so a wave whose spectrum characteristics fit the bridge site well should be used. The beam temperature difference can affect the structural seismic response, but this effect can be ignored when only considering the maximum rail seismic force. With the application of a series of three continuous beams on the arch and the reasonable arrangement of fixed bearings and speed locks, the track longitudinal stress deformation during an earthquake outperforms that of supported beams.

Keywords: railway arch bridge; track–bridge interaction; continuous welded track; longitudinal seismic response

1. Introduction

The technology developed for continuous welded rail (CWR) on bridges is one of the core technologies in modern railway tracks, providing support for high-speed and heavy load railway transportation [1–3]. However complicated operation environments and potential natural hazards provide challenges to railway safety and long-term reliable operation. In cases of earthquake damage from across the globe, railway have suffered varying degrees of damage [4–7]. The impact of earthquakes on CWR on bridges has thus gradually attracted increased attention. According to previous research (based on longitudinal track–bridge interactions), the rail longitudinal force (which is closely related to line stability, rail bar design, rail creep, and the track safety) under seismic loading is several times larger than that resulting from temperature changes. Therefore, the effect of seismic on track–bridge longitudinal response should be considered when designing CWR on bridges in seismically active zones.

In existing research on the seismic response of CWR on bridges, the natural vibration characteristics and seismic response of the bridge were shown to be affected by the longitudinal restraint of the track. Toyooka et al. conducted numerical analyses to assess the effect of the track structure on the seismic behavior of an isolated bridge, and the results proved that supplemental damping introduced by the track structure is not negligible [8]. Maragakis et al. tested natural bridge frequency and the effects of track structure on the dynamic characteristics of the bridge. The test results show that when the track structure exists, the vibration transfer from rail to embankment is more obvious. After cutting off the rail, the fundamental longitudinal, horizontal, and vertical frequency of the entire bridge structure are reduced [9]. The seismic responses of continuously welded ballasted track on bridges through the shaking table test were conducted, and the results indicated that track constraint can improve the low order natural frequency of bridges significantly, and reduce the displacement response [10]. Yan analyzed the seismic response of high-speed railways on small span simply-supported beam bridges [11]. Esmaeili developed a finite element model for a seismic analysis of ballasted railway track, and the ballast layers were modeled using a series of lumped masses connected by springs and dashpots to simulate the ballast longitudinal resistances [12]. Davis et al. [13] analyzed the earthquake excitation response of multi-span ballasted track supported by simply beam bridges via the plain, V-valley, and slope areas. The results showed that the nonlinear interaction between the beam and track must be considered when it comes to railroad bridge seismic response analysis. Fitzwilliam [14] simulated the rail–structure interaction of a ballasted track when subject to a train braking load and a seismic load. Petrangeli et al. [15] analyzed the seismic response of simply supported beam bridges under different bearing stiffness conditions. The results showed that after considering the rail constraints, the fixed support displacement can be reduced 30–60%, while the greatest rail axial force is much lower than the critical value of the loss of stability. Iemura et al. [16] designed and implemented the shaking table model test in the laboratory to study the effect of track restraints on bridge seismic response.

Published research reveals that the stress deformation mechanism of CWR track on large-span arch bridges is complex and quite different from that of simply supported beam bridges and continuous beam bridges. However, previous work on track–bridge interaction under uniform seismic excitation mainly focuses on the seismic response of simply supported beam bridges and continuous beam bridges. It fails to fully account for the seismic response of CWR track on large-span arch bridges. Consequently, it is necessary to further analyze the longitudinal seismic response of CWR on arch bridges to quantitatively predict seismic behavior in different scenarios. In addition, in recent mountain railway construction in China, large-span arch bridges have been frequently utilized [17,18]; the bridge sites are in dangerous areas and across river valleys, where the probability of earthquakes is greater. The seismic responses of CWR track on arch bridge is yet to be demonstrated.

Based on the discussion above, the research presented here aims at identifying the longitudinal stress deformation mechanism of CWR tracks on arch bridges under seismic loading. In particular, an integrated track–bridge spatial coupling finite element model was established and a nonlinear spring element was used to simulate track–bridge contact. The study included an investigation of the effect that seismic loading has on rail longitudinal force, pier top displacement, and dynamic characteristics of track resistance. The effect of seismic excitations, thermal changes, bridge span layout, and changes to other parameters were compared.

2. Calculation Model for CWR Seismic Response on Deck Arch Bridges

The finite element simulation technique is a relatively mature and widely adopted method for discussing the seismic response of CWR on bridges [12,15]. An integrated track–bridge spatial coupling finite element model was established, taking into consideration detailed structural features of the arch bridge (including the distribution of mass and stiffness of ribs, web members, longitudinal bracing rods, and cross ties), so as to obtain a system stiffness and mass matrix similar to the actual structure.

2.1. Numerical Model

We developed a numerical model of CWR on bridges. The junction piers at both ends are relatively high and pier mass distribution has a great impact on the structural dynamic characteristics, so the actual pier structure should be considered when modelling with beam elements [17]. In particular, secondary dead loads of the bridge deck (including ballast/track slabs, sleepers, rails, fasteners, sidewalk slabs) were simplified into a quality system longitudinally evenly distributed along the beam surface.

To include the influence of the track on the seismic response of the bridge, a vertical spring was introduced that simulated the vertical stiffness of the track, and an elastic-plastic spring element was used to simulate the longitudinal resistance of the track [19]. The dynamic hysteresis curve of the spring element is shown in Figure 1, in which F_{j} is the longitudinal resistance of the track and δ_{j} is the track–bridge relative displacement.

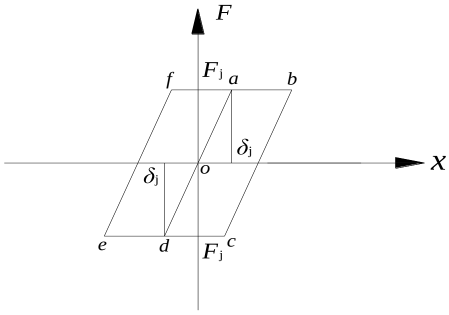

Figure 1. Hysteresis of resistance spring element.

In addition, outside of the bridge, the track together with 100 m of the embankment was simulated, in order to reduce the influence of the boundary conditions and to accurately simulate the track–bridge interaction. The finite element model is shown in Figure 2. From a practical point of view, the orthogonal damping model-Rayleigh method was adopted [20,21]. The structural vibration equation under seismic loading can be expressed as

$$[M]\{\ddot{x}(t)\} + [C]\{\dot{x}(t)\} + [K]\{x(t)\} = -[M][I]\{\ddot{x}_{\mathrm{g}}(t)\} \tag{1}$$

where [M], [C], and [K] refer to the mass matrix, damping matrix, and stiffness matrix of the system respectively; $\{\ddot{x}(t)\}$, $\{\dot{x}(t)\}$, and $\{x(t)\}$ refer to the acceleration, speed, and displacement time interval in relation to the subgrade ground, respectively; $[I]$ refers to the influence matrix; and $\{\ddot{x}_g(t)\}$ refers to the seismic wave acceleration time interval within the subgrade ground. The damping matrix can be expressed based on the Rayleigh method as

$$[C] = \alpha[M] + \beta[K] \tag{2}$$

where α and β refer to the mass damping coefficient and stiffness damping coefficient respectively. They can be calculated based on the damping ratios as

$$\alpha = \frac{2\omega_{\mathrm{i}}\omega_{\mathrm{j}}(\xi_{\mathrm{i}}\omega_{\mathrm{j}} - \xi_{\mathrm{j}}\omega_{\mathrm{i}})}{\omega_{\mathrm{j}}^2 - \omega_{\mathrm{i}}^2} \tag{3}$$

$$\beta = \frac{2(\xi_{\mathrm{j}}\omega_{\mathrm{j}} - \xi_{\mathrm{i}}\omega_{\mathrm{i}})}{\omega_{\mathrm{j}}^2 - \omega_{\mathrm{i}}^2} \tag{4}$$

where ω_{i} and ω_{j} refer to the natural frequencies of the *i*th and *j*th order of the structure, respectively; ξ_{i} and ξ_{j} refer to the damping ratios in relation to the *i*th and *j*th order, respectively. In regards to the test detailed in this paper, the longitudinal first-order natural frequencies of the long and short beams were calculated. When discussing the dynamic response of CWR on bridges, the damping coefficient is usually calculated by selecting the natural vibration frequency of the relevant vibration mode. The damping ratio of a concrete bridge is generally 0.02–0.05, and for a steel bridge it is generally 0.02–0.03. In this paper, the former two-class nature frequency of the system were taken and the damping ratio was taken to be 0.05. The damping coefficients α and β were taken to be

$$\alpha = 2\frac{0.05\omega_1\omega_2}{\omega_1+\omega_2},\ \beta = 2\frac{0.05}{\omega_1+\omega_2}\ . \tag{5}$$

The analysis was based on the Newmark-β method and the integral parameters used for the calculation are γ = 0.5 and β = 0.25 respectively.

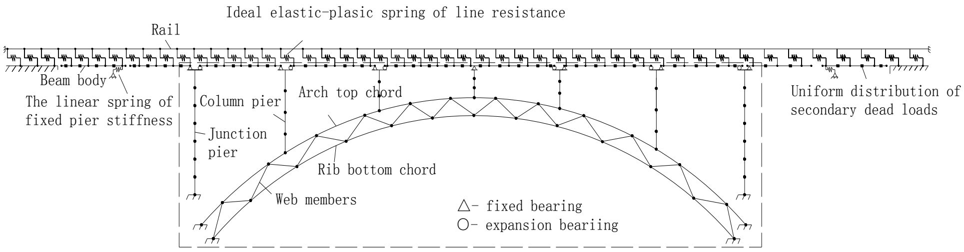

Figure 2. Track-arch bridge interaction finite element model.

2.2. Project Description

2.2.1. Bridge Overview

The static arrangement of the arch bridge were (1 × 24 m + 4 × 32 m) with simple supporting beams, a 1 × 352 m steel truss arch and 8 × 32 m simple supporting beams. The deck length was 352.0 m, and the height was 64.5 m, as shown in Figure 3. The piers were numbered from left to right P1, P2, . . . P29, of which P6 and P21 piers are the left and right junction piers, and P7–P20 are the arch column piers.

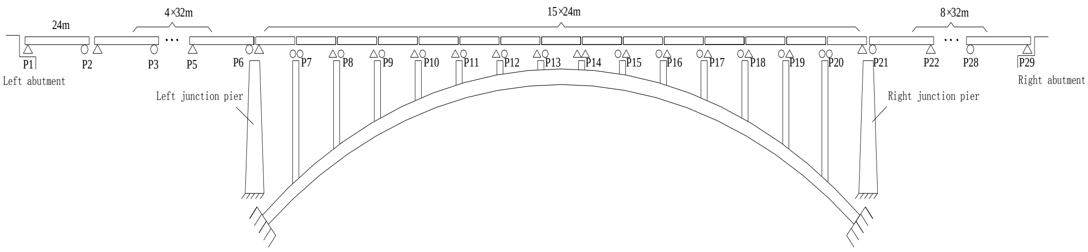

Figure 3. Bridge span layout.

The parameters of the 24 m and 32 m simply supported beams are given in Table 1 below.

Table 1. Parameters of 24 m and 32 m simply supported beams.

Bridge Span (m)	Beam Cross-Sectional Area (m^2/line)	Sectional Moment of Inertia (m^4/line)	Distance from Section Core to the Upper Edge (m)	Distance from Section Core to the Lower Edge (m)	Beam BODY Weight (t)	Secondary Dead Load (kN/m)
24	2.60	1.54	0.80	1.30	197.88	74.68
32	2.92	2.69	0.94	1.56	279.30	

The rail consisted of CHN60, type-III concrete sleepers with a type-II fastener system. The longitudinal force-displacement relationship is expressed as [22]

$$f = \begin{cases} 7.5u, |u| \le 2\text{ mm} \\ 15, |u| \ge 2\text{ mm} \end{cases} \tag{6}$$

where f represents the longitudinal resistance of track (unit: kN/m per rail); and u represents the longitudinal relative displacement between track and bridge (unit: mm).

The temperature difference for concrete beam was 15 °C [22]. Since there are no previous estimates on rib temperature difference, the temperature difference of ballasted steel beams (25 °C) was also applied to the ribs. The column piers and cap beams were assumed to have the same value as the ribs.

2.2.2. Selection of Seismic Waves

The calculations presented here require seismic waves as input, in order to explore the seismic response characteristics of continuously welded ballasted track on arch bridges. From among the existing recorded seismic waves, the El-Centro seismic wave (USA, 1940, NS), San Fernando (1971) seismic wave and James RD (1979) seismic wave were selected as inputs for ground motions in the model [10] (as shown in Figure 4), with characteristic periods of 0.66 s, 0.28 s, and 0.46 s, respectively. When discussing the dynamic response of continuously welded ballasted track on arch bridges under seismic loading, the acceleration peak values were set to 0.4 g.

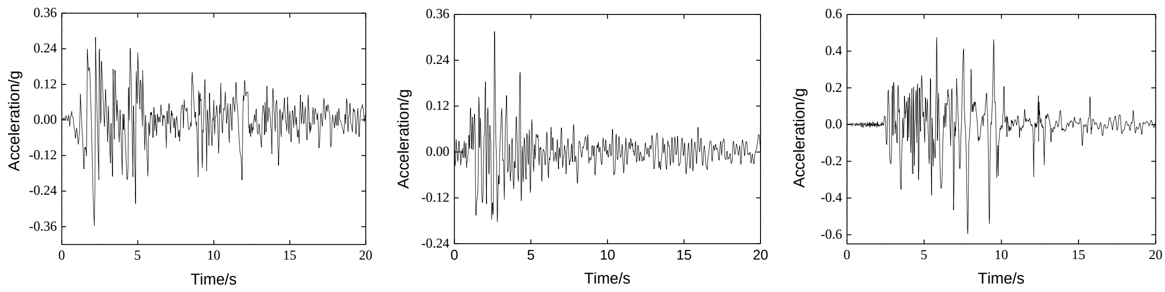

(**a**) (**b**) (**c**)

Figure 4. Three seismic waves. (**a**) El-Centro wave; (**b**) San Fernando wave; (**c**) James RD wave.

3. Influence of Track Constraints on Arch Bridge Seismic Response

The seismic response of deck arch bridges with and without track constraints were calculated, taking the uniform longitudinal input by El-Centro wave excitation as an example. The analysis focused of structural deformation and the symmetry of bridge structures, thus the pier top displacement responses of the left junction pier and left-span column piers (piers P6~P13 in Figure 3) were compared. This paper also focuses on the effect of seismic activity on track–bridge longitudinal response for CWR on bridges in a seismically active zone. The influence of live train loads is not yet clear and should be the subject of further research.

3.1. Comparison of Rail Seismic Force

The analysis focused on longitudinal seismic vibrations. According to existing research based on longitudinal track–bridge interactions, the force under seismic loading is several times larger than that due to temperature change [12,15]. Therefore, the seismic effect on rail longitudinal forces should be considered when designing CWR on bridges in seismically active zones. Compared with vertical and transverse seismic vibrations, longitudinal seismic vibrations have the most direct and important effect on rail longitudinal force. The longitudinal force distribution of our track model is shown in Figure 5.

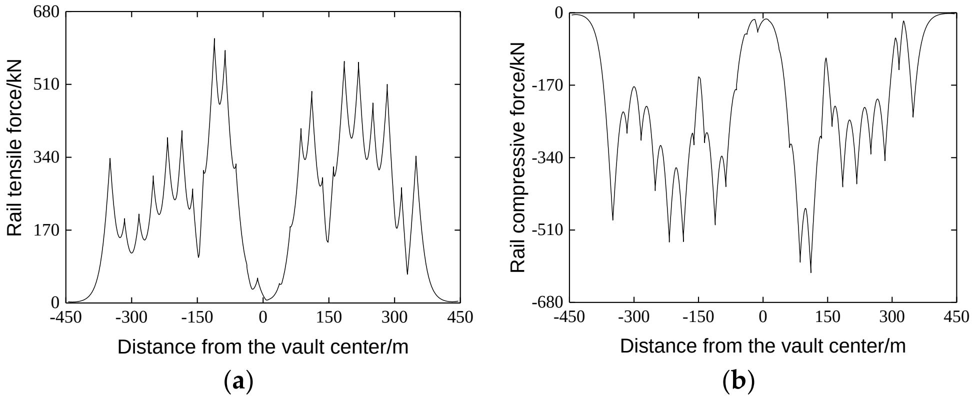

Figure 5. Longitudinal rail force envelope. (**a**) Tensile force; (**b**) compressive force.

As seen in Figure 5, the peak rail seismic forces occur in the vicinity of the beam gap, which is similar to estimates of rail expansion force in regular calculations. The seismic force on the span of a simply supported beam at the arch center is the least, up to about 50 kN. This indicates that the track structure at the arch center is least prone to instability or damage when an earthquake occurs. When calculating the calculated rail expansion force, the 'maximum rail seismic force' was taken to be the maximum absolute value of the tensile/compressive rail seismic force under unidirectional input of seismic waves. The peak rail seismic force (617.3 kN) is larger than the maximum expansion force (568.7 kN, see Figure 6); the latter was calculated according to existing codes for CWR tracks on bridges [17]. This reinforces the importance of a study of seismic impact on CWR track on bridges.

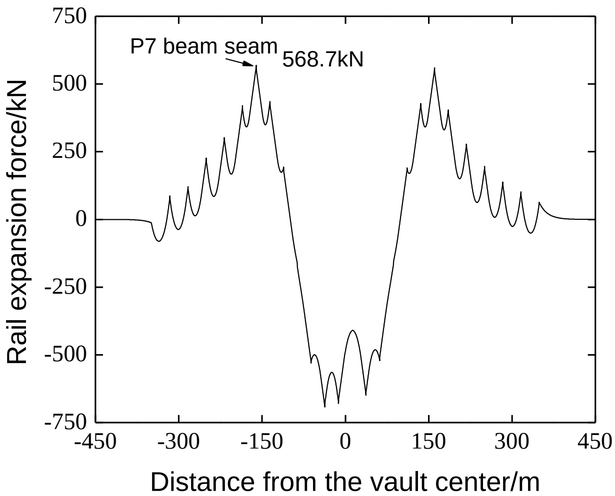

Figure 6. Rail expansion force.

3.2. Comparison of Pier Top Displacement

Pier top displacement was used to assess the effect of seismic activity. Given the huge amount of data generated from the models, only the highest pier column, P7, is used as an example. The pier top longitudinal displacement over time is shown in Figure 7a, and the maximum displacement of each pier top is shown in Figure 7b below.

As shown in Figure 7, when the track constraints were considered in the calculation for a deck arch bridge, the pier top longitudinal displacement under seismic action was greatly reduced. In Figure 7b, the maximum pier top longitudinal displacements of piers P6–P13 were 14.6, 9.6, 8.1, 15.0, 22.8, 22.8, 23.7, and 24.2%, respectively—obtained when no track constraints were considered. In the analysis of simply-supported beam bridges, the pier top displacements were about 19–62% when no track constraints were considered [17]. This is chiefly because the arch bridge pier column stiffness is generally less than the average pier stiffness; while the constraint of the track longitudinal resistance on beams in an the arch bridge is greater than that of supporting beam bridges, resulting in significant reduction in pier top displacement. Since the column pier deformation directly affects the structural forces (such as pier shear and bending moment, rib axial force and bending moment, etc.), it is proposed that track constraints should be taken into consideration in railway arch bridge seismic design.

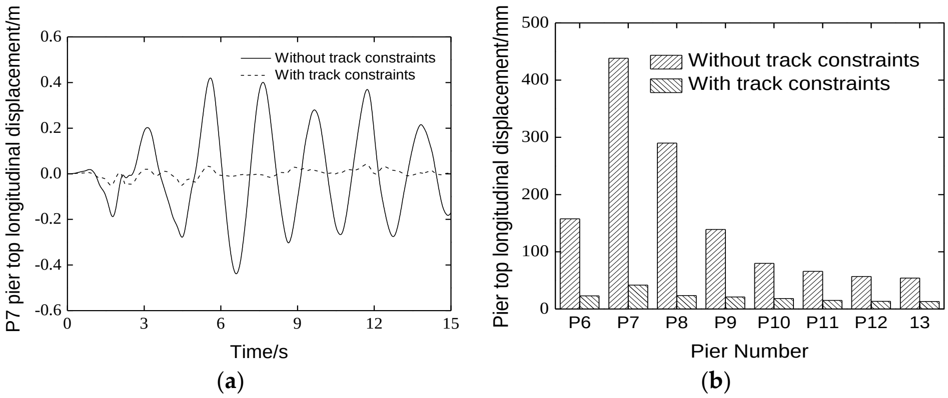

Figure 7. Comparison of pier top longitudinal displacement. (**a**) P7 pier top displacement; (**b**) the maximum pier top displacement.

3.3. Dynamic Characteristics of Track Resistance

The dynamic hysteretic force–displacement curves for track resistance near the pier column P7 and the arch center are plotted in Figure 8.

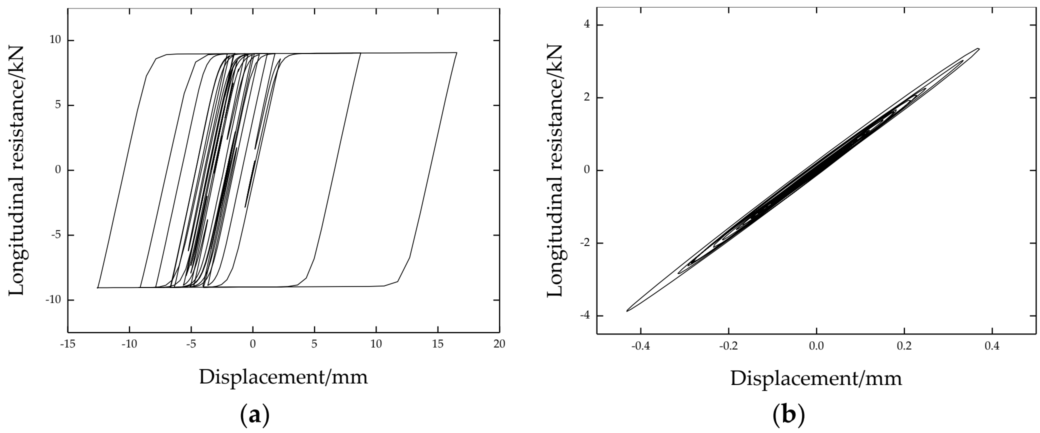

Figure 8. Hysteresis curves of track resistance. (**a**) P7 pier column; (**b**) arch center.

As demonstrated in Figure 8, the track resistance–displacement hysteretic curve coincides well with the elastic–plastic resistance in Figure 1, and the value of the yielding force is the maximum force transmissible by a single track resistance element. In particular, it can be seen from Figure 8a that the area surrounded by the hysteresis curve increases gradually with the increase in dynamic displacement. Under seismic loading, the track constraints can be considered to be in a relatively stable state of energy dissipation. In addition, the hysteresis curve of track resistance near the arch center is spindle shaped, indicating that it is ductile.

In addition, the force-displacement curves of track resistance under seismic loading are a set of closed and relatively stable hysteretic curves. The shape of the hysteretic curves is basically the same with the Bouc–Wen model [23], however, in consideration of the strong nonlinearity of track-bridge interaction and structural dynamic response, the track longitudinal resistance has significant nonlinear characteristics. In particular, the track longitudinal load-bearing and force-transference mechanisms are highly complex because of the discreteness of the track structures and repeatability of loads. Thus, the parameters used for the skeleton curve and family of ballast hysteretic curves/models are differenced under different loading conditions [24,25]. At present, this paper mainly focuses on longitudinal seismic response of CWR on arch bridge by adopting ideal elastic–plastic hysteretic models, and the influence of phenomenological models yet to be clarified.

4. Influential Factors of Seismic Response on CWR on Arch Bridge

In this section, the impact of the seismic wave spectrum, beam temperature difference, and bridge span layout on the rail seismic force are analyzed.

4.1. Seismic Wave Spectrum

The rail seismic forces under El-Centro, San Fernando, and James RD waves are compared in Figure 9. It can be seen that, under the same peak acceleration, the maximum rail seismic force under San Fernando waves increases by 71.6% compared with El-Centro waves—up to 1059.4 kN. The maximum rail seismic force under James RD waves increases by 147.5% and 44.2% as compared with El-Centro and San Fernando waves respectively—up to 1527.7 kN. This indicates that the seismic wave spectrum characteristics exert great impact on the seismic response of arch bridges. According to the existing research, the maximum allowable rail longitudinal force is about 1500 kN (the safety factor is 1.3) [22]. For the San Fernando wave, the maximum rail longitudinal force could be up to 1628.7 kN, when accompanied by a rise in rail temperature of 30 °C. For James RD waves, the maximum rail longitudinal force might exceed 1500 kN, regardless of the temperature rise. The track stability may not be guaranteed under these two cases, which should be control conditions for the design of CWR track on bridge. These cases demonstrate the significance of seismic action for the design of CWR track on bridges in earthquake zones.

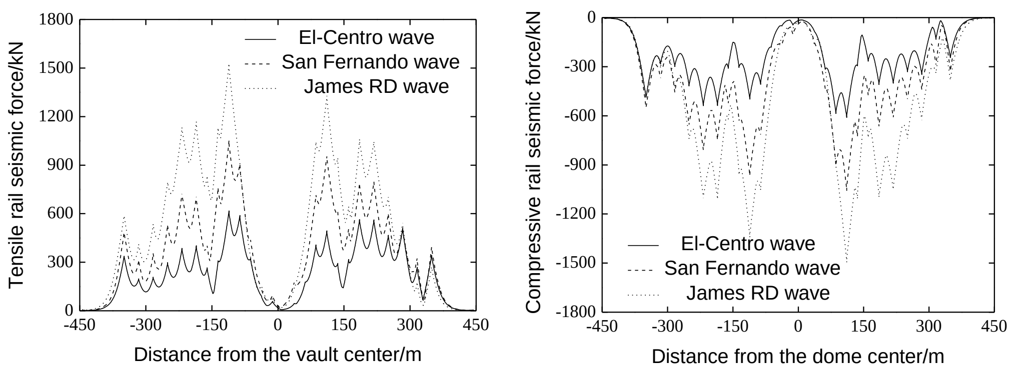

(**a**) (**b**)

Figure 9. Rail seismic force comparison. (**a**) Tensile force; (**b**) compressive force.

The effect of seismic forces on CWR tracks on arch bridges varies greatly under different seismic waves. To avoid potentially large calculation errors, seismic waves consistent with the spectrum features of bridge site should be used for analysis. In the following section, only San Fernando wave input is used; the role of longitudinal force of CWR tracks on arch bridges has already been highlighted above.

4.2. Rib Temperature Difference

The above calculations are based on zero additional rail force, however earthquakes take place occasionally and a very large additional force might accumulate in the rail before an earthquake.

The influence of the expansion force caused by rib temperature difference cannot be ignored. In this section, the rib temperature differences were taken to be 5, 15, and 25 °C.

Taking the temperature difference of 25 °C as an example, the rail force at the beam gaps of piers P7 and P9 at different times are shown in Figure 10.

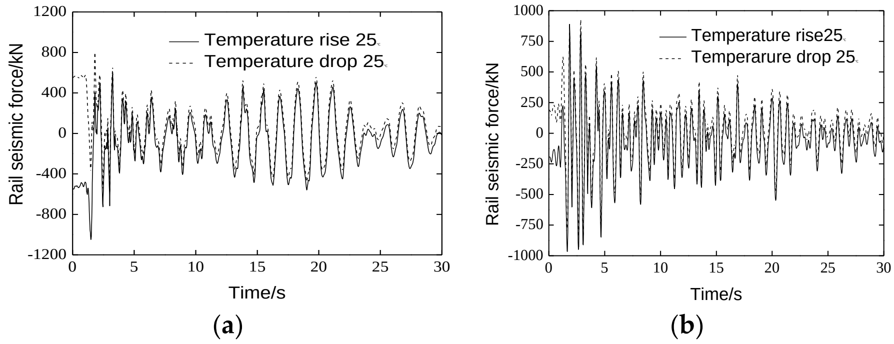

Figure 10. Rail seismic force time history at temperature change. (**a**) Pier P7 beam gap; (**b**) pier P9 beam gap.

Figure 10 shows that the longitudinal forces were 568.7 kN and 193.8 kN at the beam gap of piers P7 and P9 (obtained from Figure 6) before the earthquake. Subsequently, beam displacement caused by seismic action led to redistribution of rail longitudinal force. Within 2 s of the earthquake, the rail seismic forces changes very significantly and the values are very different depending on whether we consider a temperature rise or fall of the ribs. In the subsequent vibration process, the difference is insignificant for the two conditions as the rail expansion force might be released to a great extent. The maximum rail seismic forces at all beam gaps from the left junction pier P6 to right junction pier P21 with different rib temperature changes are compared in Figure 11.

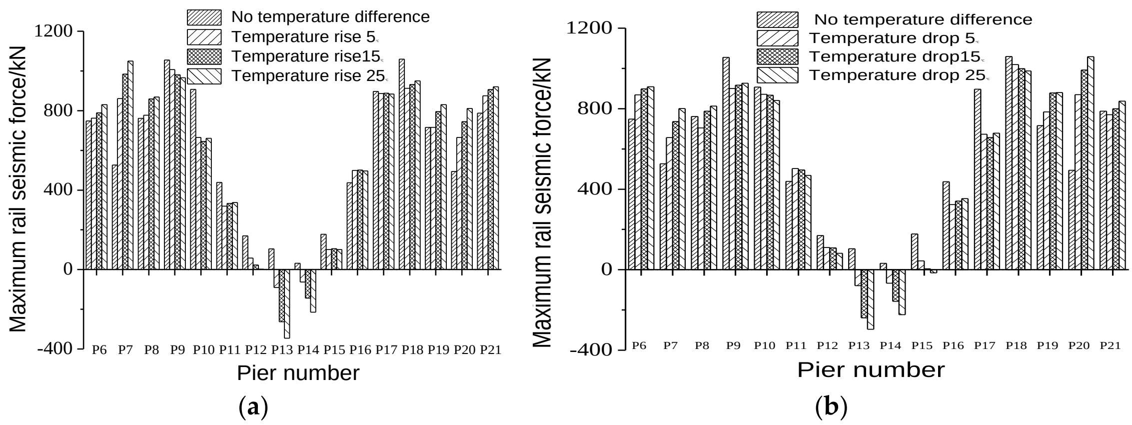

Figure 11. Maximum seismic force at beam gaps. (**a**) Temperature rise; (**b**) temperature drop.

As shown in Figure 11, notwithstanding the difference in rail seismic force at various beam gaps, the forces at temperature changes of 5, 15, and 25 °C were 1018.8, 998.6, and 1058.4 kN, respectively, with only minor difference compared to no temperature change. The effect of rib temperature change can be ignored if only considering the maximum rail seismic force. At a rib temperature change of 25 °C, the distribution of additional longitudinal rail force after an earthquake is shown in Figure 12.

As shown in Figure 12, due to the release and redistribution effects of an earthquake on rail expansion force, the peaks of rail expansion force at beam gap were much reduced. The maximum additional longitudinal rail forces were only 106.6 kN and 118.8 kN after an earthquake after a temperature rise and fall respectively.

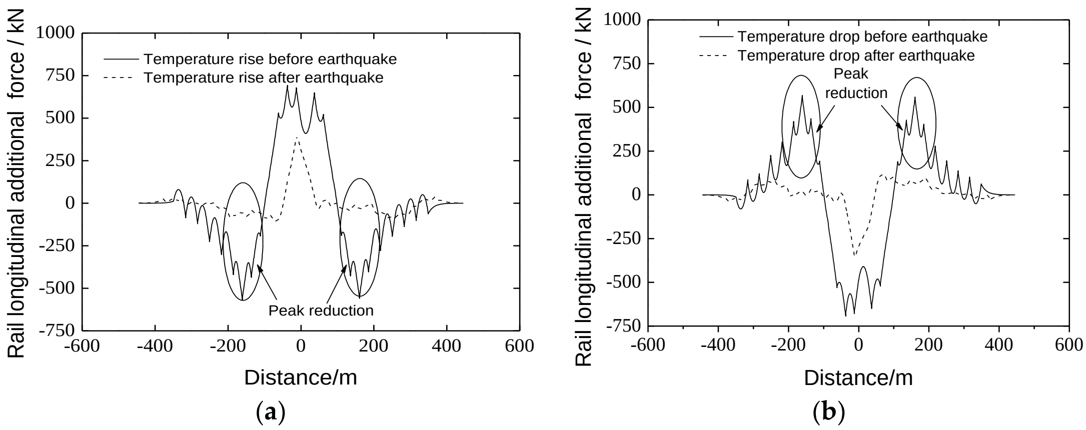

Figure 12. Additional longitudinal rail force after earthquake. (**a**) Temperature rise; (**b**) temperature drop.

4.3. Bridge Span Layout

It is noted that the track force and deformation under expansion, deflection, and other conditions for arch bridges with continuous beams outperformed those of simply supported beams bridges [17]. In this section, the impact of bridge span layout on rail seismic force was analyzed by comparing three options and the original proposal (simply supported beam bridges on the arch).

Option 1: A series of three 5 × 24 m continuous beams on the arch with the fixed bearings of two outer continuous beams at the junction piers, as shown in Figure 13a.

Option 2: Based on option one with speed locks on column piers P11, P13, and P16, as shown in Figure 13b.

Option 3: Based on option two, with speed locks on column piers P10 and P17, as shown in Figure 13c.

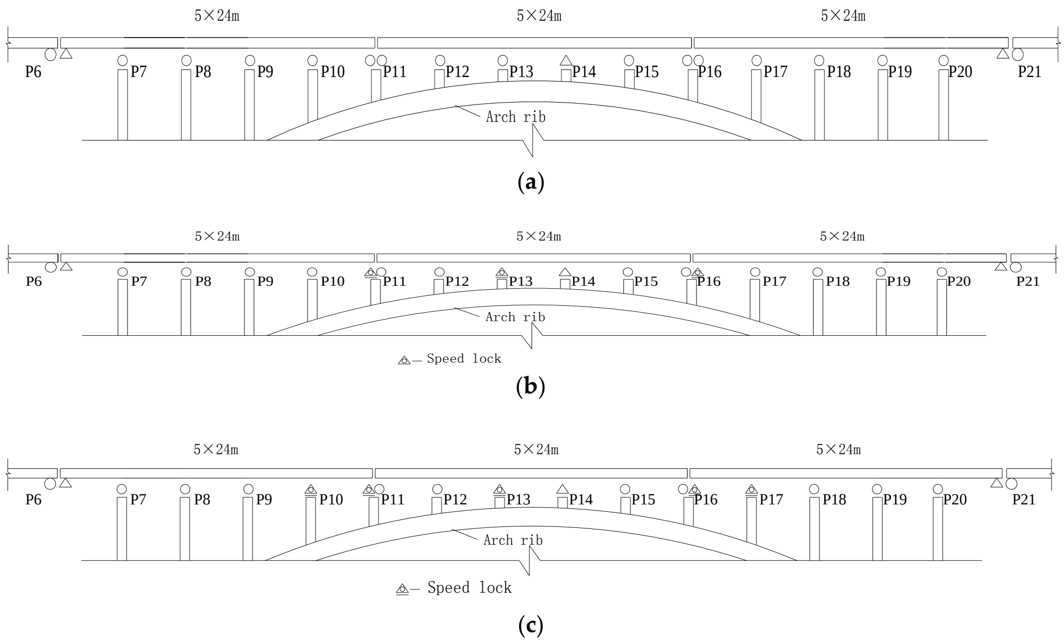

Figure 13. Options of bridge span layout. (**a**) Option 1; (**b**) option 2; (**c**) option 3.

The comparison of rail seismic force is shown in Figures 14 and 15.

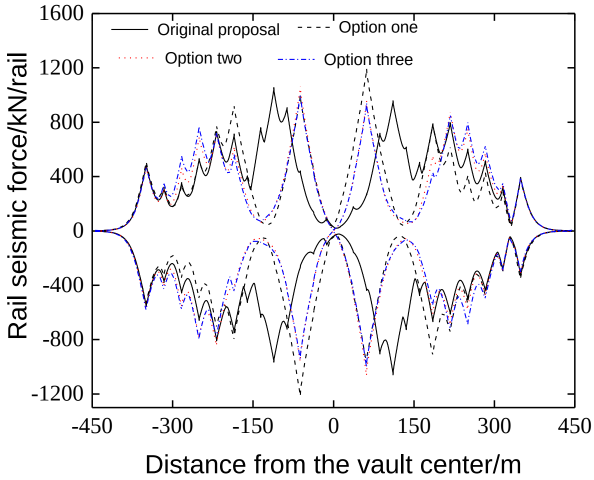

Figure 14. Rail seismic forces.

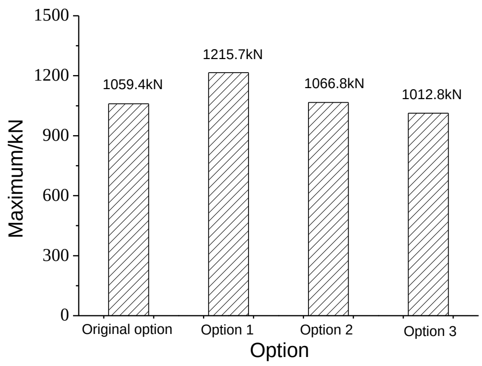

Figure 15. Maximum rail seismic force for each option.

As shown in Figures 14 and 15, the maximum rail seismic force was 1215.7 kN in option one, an increase of 156.3 kN from the original proposal. By setting speed locks, the maximum seismic forces were effectively reduced in options 2 and 3, by 1066.8 kN and 1012.8 kN respectively, similar or even slightly smaller than the original proposal. The application of additional speed locks thus further reduced the rail seismic force, mainly because the application of a series of three continuous beams on the arch minimized the effect of rib deformation on beam displacement.

5. Conclusions

This paper presents the seismic response of CWR on arch bridges. The major results can be summarized as follows:

(1) Track constraints need to be considered in seismic calculations, or structural seismic response will be overestimated. When the track constraints were considered in the calculation for a deck arch bridge, the pier top longitudinal displacement under seismic action was greatly reduced. The peak rail seismic force is larger than the maximum expansion force calculated according to existing codes for CWR tracks on bridges, which reinforces the importance of a study of seismic impact on CWR track on bridges.

(2) The rail seismic forces change very significantly and the values are very different depending on whether we consider a temperature rise or fall of the ribs. The effect of rib temperature change can be ignored if only considering the maximum rail seismic force.

(3) With the application of a series of three continuous beams on the arch and the reasonable arrangement of fixed bearings and speed locks, the maximum seismic forces were effectively

reduced, which is mainly because the application of a series of three continuous beams on the arch minimized the effect of rib deformation on beam displacement.

(4) This paper also focuses on the effect of seismic activity on track–bridge longitudinal response for CWR on bridges in a seismically active zone. The influence of live train loads and phenomenological resistance models is yet to be clarified, and should be the subject of further research.

Author Contributions: J.X. and R.C. conceived the method; X.W. built the mathematical model and analyzed the results; H.L. wrote the paper. P.W. supervised the entire work; X.W. and J.X. wrote part of code.

Acknowledgments: The present work has been supported by the National Natural Science Foundation of China (51425804, 51778542, and U1734207), and the Doctorial Innovation Fund of Southwest Jiaotong University (No. 2014310016).

Conflicts of Interest: The authors declare that there is no conflict of interests regarding the publication of this paper.

References

1. Esveld, C. *Modern Railway Track*, 2nd ed.; MRT-Productions: Zaltbommel, The Netherlands, 2001.
2. Ruge, P.; Bike, C. Longitudinal forces in continuously welded rails on bridge decks due to nonlinear track bridge interaction. *Comput. Struct.* **2007**, *85*, 458–475. [CrossRef]
3. Chen, R.; Wang, P.; Wei, X.K. Track-bridge longitudinal interaction of continuous welded rails on arch bridge. *Math. Probl. Eng.* **2013**. [CrossRef]
4. Domaneschi, M.; Martinelli, L.; Po, E. Control of Wind Buffeting Vibrations in a Suspension Bridge by TMD: Hybridization and robustness issues. *Comput. Struct.* **2015**, *155*, 3–17. [CrossRef]
5. Domaneschi, M.; Limongelli, M.P.; Martinelli, L. Damage detection and localization on a benchmark cable-stayed bridge. *Earthq. Struct.* **2015**, *8*, 1113–1126. [CrossRef]
6. Zhu, Y.; Wei, Y.X. Characteristics of Railway Damage due to Wenchuan Earthquake and Countermeasure Considerations of Engineering Seismic Design. *Chin. J. Rock Mech. Eng.* **2010**, *29*, 3378–3386.
7. Sogabe, M.; Asanuma, K.; Nakamura, T.; Kataoka, H.; Goto, K.; Tokunaga, M. Deformation Behavior of Ballasted Track during Earthquakes. *Q. Rep. RTRI* **2013**, *54*, 104–111. [CrossRef]
8. Toyooka, A.; Ikeda, M.; Yanagawa, H.; Kataoka, H.; Iemura, H.; Murata, K. Effect of Track Structure on Seismic Behavior of Isolation System Bridges. *Q. Rep. RTRI* **2005**, *46*, 238–243. [CrossRef]
9. Maragakis, E.; Douglas, B.; Chen, Q.B.; Sandirasegaram, U. Full-scale Tests of a Railway Bridge. *Transp. Res. Rec. J. Transp. Res. Board* **1998**, *1624*, 140–147. [CrossRef]
10. Wang, P.; Liu, H.; Wei, X.K.; Chen, R.; Xiao, J.L.; Xu, J.M. Shaking table testing and numerical modeling of continuous welded ballast track on bridges under longitudinal seismic loading. *J. Vibroeng.* **2017**, *19*, 3610–3628. [CrossRef]
11. Yan, B.; Liu, S.; Pu, H.; Dai, G.L.; Cai, X.P. Elastic-plastic seismic response of CRTSII slab ballastless track system on High-speed railway bridges. *Sci. China Technol. Sci.* **2017**, *60*, 865–871. [CrossRef]
12. Esmaeili, M.; Noghabi, H.H. Investigating seismic behavior of ballasted railway track in earthquake excitation using finite-element model in three-dimensional space. *J. Transp. Eng.* **2013**, *139*, 697–708. [CrossRef]
13. Davis, S.G. *Track-Structure Interaction in Seismic Conditions, Track–Bridge Interaction on High-Speed Railways*; Taylor & Francis Group: London, UK, 2007; pp. 29–35.
14. Fitzwilliam, D. Track structure interactions for the Taiwan High Speed Rail project. *IABSE Symp. Rep. Int. Assoc. Bridge Struct. Eng.* **2003**, *87*, 73–79. [CrossRef]
15. Petrangeli, M.; Tamagno, C.; Tortolini, P. Numerical analysis of track: Structure interaction and time domain resonance. *Proc. Inst. Mech. Eng. Part F J. Rail Rapid Transit* **2008**, *222*, 345–353. [CrossRef]
16. Iemura, H.; Iwata, S.; Murata, K. Shake table tests and numerical modeling of seismically isolated railway bridges. In Proceedings of the 13th World Conference on Earthquake Engineering, Vancouver, BC, Canada, 1–6 August 2004; Volume 1780, pp. 1–15.
17. Wei, X.K. Research on Longitudinal Interaction between Girder and Track Seismic Response Analysis of Continuous Welded Rail on Arch Bridge. Ph.D. Thesis, Southwest Jiaotong University, Chengdu, China, 2014.
18. Wang, P.; Xiao J, L.; Chen, R.; Tian, C.X. *Technology of Continuous Welded Rail on Bridges for High-Speed Railway*; China Railway Publishing House: Beijing, China, 2016.

19. Yan, B.; Dai, G.L. Seismic Pounding and Protection Measures of Simply-Supported Beams Considering Interaction between Continuously Welded Rail and Bridge. *Struct. Eng. Int.* **2013**, *23*, 61–67. [CrossRef]
20. Liu, W.S. Track-Bridge Interaction between Continuous Welded Rail and Long-Span Stress-Truss Arch Bridge of High-Speed Rails. Ph.D. Thesis, Central South University, Changsha, China, 2013.
21. Newmark, N.M. Method of computation for structural dynamics. *J. Eng. Mech. Div.* **1959**, *85*, 67–94.
22. China Railway. *TB10015-2012, Code for Design of Railway Continuously Welded Rail*; China Railway Publishing House: Beijing, China, 2012.
23. Domaneschi, M. Simulation of Controlled Hysteresis by the Semi-active Bouc-Wen Model. *Comput. Struct.* **2012**, *106–107*, 245–257. [CrossRef]
24. Liu, H.; Xiao, J.L.; Wang, P.; Liu, G.Z.; Gao, M.Y.; Li, S.Z. Experimental investigation of the characteristics of a granular ballast bed under cyclic longitudinal loading. *Constr. Build. Mater.* **2018**, *163*, 214–224. [CrossRef]
25. Xiao, J.L.; Liu, H.; Xu, J.M.; Wang, P.; Liu, G.Z.; Chen, R. Longitudinal resistance performance of granular ballast beds under cyclic symmetric displacement loading. *J. Zhejiang Univ.-Sci A* **2017**, *18*, 648–659. [CrossRef]